AIAA JOURNAL
Vol. 31, No. 3, March 1993

Flowfield Measurements of a Two-Element Airfoil with Large Separation

Kasim Biber* and Glen W. Zumwalt†
Wichita State University, Wichita, Kansas 67260

Detailed measurements of moderate to large separated flows have been made for the 13%-thick GA(W)-2 airfoil with 25% slotted flap at a Reynolds number of 2.2×10^6 and Mach number of 0.13. The tests were made for flap nested and flap deflected cases of 30- and 40-deg flap angles with optimum and narrow gaps at near- and poststall angles of attack. The data include pressure, mean flow, and turbulence quantities. A splitter plate was employed for measuring a large number of static pressures simultaneously. Flowfield sensitivity to the measuring probes was determined by means of force and surface pressure measurements. The experimental program revealed the difficulty of measuring pressures in separated flows. The presence of a probe, no matter how small, changes the flow geometry in the interacting parts of the flowfield. The results of this experimental study are sufficiently detailed to serve to evaluate computational codes of such separated flows on multielement airfoils.

Nomenclature

C_d	= drag coefficient
C_l	= lift coefficient
$C_{l_{max}}$	= maximum lift coefficient
C_m	= pitching moment coefficient
C_p	= static pressure coefficient, $\equiv (p - p_\infty)/q_\infty$
C_{p_T}	= total pressure coefficient, $\equiv (p_T - p_\infty)/q_\infty$
c	= mean chord, $\equiv 0.61$ m (2 ft) for the GA(W)-2 airfoil
G/c	= gap-to-chord ratio
O/c	= overlap-to-chord ratio
p	= local static pressure
p_T	= local total pressure
p_∞	= free-stream static pressure
q_∞	= indicated dynamic pressure, $\equiv 1150$ N/m^2 (24 psf)
U_{ref}	= tunnel freestream reference velocity (U_∞)
U, V	= mean flow velocity components
u, v	= instantaneous flow velocity components
u', v'	= fluctuating flow velocity components
$\overline{u'^2}, \overline{v'^2}$	= Reynolds normal stress components
$\overline{u'v'}$	= Reynolds shear stress
V_{tot}	= total mean flow velocity, $\equiv \sqrt{U^2 + V^2}$
X, Y	= tunnel coordinates: X is along the tunnel centerline (positive downstream) and Y is vertical (positive upward)
x, y	= airfoil coordinates: x is along the chord line
α	= angle of attack
δ	= flap deflection angle

Introduction

THE flow mechanism on multielement airfoils differs from that on single-element airfoils by the complexity of the flowfield introduced by the flap deployment. The presence of confluent boundary layers, cove separation bubble, off the surface pressure recovery, strong viscous-inviscid interactions, and pressure gradients across the wake characterize the distinctive features of the flow around multielement airfoils. When the flow separates from the upper surface, the unsteady circulatory motion inside the separated wake makes the flow even more complicated to deal with. Figure 1 shows such separated flowfield with its interacting parts. Sufficient knowledge of this flow mechanism is essential in multielement airfoil design and performance predictions. This is why there have been numerous computational and experimental investigations on multielement airfoils since they were first used in high-lift generation.

The vast majority of experiments on multielement airfoils have been conducted for the measurements of velocity and turbulence quantities with limited pressure data, at pre- or near-stall angles of attack conditions without highly separated flow. Even if there is separation, it is on the flap at low angles of attack. The work of Ref. 1 appears to be the most detailed and extensive experimental data of this kind available, without any field pressure data, for the evaluation of computational codes, such as the one reported in Ref. 2. Velocity and turbulence data in the vicinity of a single-slotted flap has been reported in Ref. 3 for attached flow and in Ref. 4 for separated flow cases. Flowfield measurements on various high-lift configurations have been made mostly at survey stations to obtain velocity and turbulence quantities for attached and nonconfluent flow in Ref. 5, and attached and confluent flow in Ref. 6. Pressure profiles are also included in Ref. 7 for small-scale separated flow and in Ref. 8 for moderately separated flow, using point measuring pitot-static probes. However, there is still a need for experimental data for validating computational codes developed for highly separated wake models, as in Ref. 9.

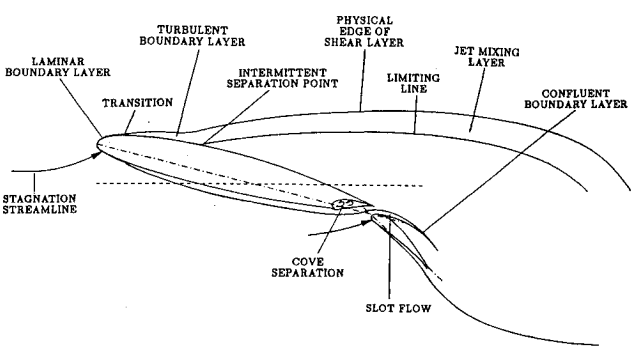

Fig. 1 Theoretical model for separated flow on a two-element airfoil.

Presented in part as Paper 92-0267 at the AIAA 30th Aerospace Sciences Meeting, Reno, NV, Jan. 6-9, 1992; received March 16, 1992; revision received June 12, 1992; accepted for publication July 13, 1992.

*Postdoctoral Fellow, National Institute for Aviation Research. Member AIAA.

†Distinguished Professor, Department of Aerospace Engineering. Associate Fellow AIAA.

The present experimental investigation is a detailed measurement of moderate to large separated flowfield on a two-element airfoil. The flowfield pressure, velocity, and turbulence quantities have been obtained using a specially designed splitter plate, a disk probe and a double-pitot tube, and an X-probe hot film anemometer, respectively. The data are intended to assist and guide the development and evaluation of computational methods for such separated flows.

Experimental Arrangement

The tests were conducted in the Wichita State University (WSU) 2.13×3.05 m (7×10 ft) wind tunnel fitted with two inserts, providing a 2.13 m (7 ft) high and 0.914 m (3 ft) wide two-dimensional test section. The test model used was the 13%-thick GA(W)-2 airfoil with 25% single-slotted flap, having a reference chord of 0.61 m (2 ft) at flap nested position and span of 0.914 m (3 ft). The main wing terminates at 0.875c and has a cove region where the flap retracts for the single-element case. Details of tunnel, model, supporting end plates, and surface pressure taps are given in Refs. 8 and 10-12.

With the inclusion of the single-element airfoil, five different airfoil configurations, each having a different gap, were selected for the present experiments. However, in this paper, results will be presented only for typical test cases. Full results are available in Ref. 13 for the test matrix shown in Table 1. The selection of the test matrix was based on previous flap optimization studies[10,11] conducted for NASA at WSU on the GA(W)-2 airfoil model. Each flap deflected case (30 and 40 deg) had an optimum and a narrow gap. For the optimum gap, the main wing wake does not merge with the boundary layer on the flap upper surface until near the flap trailing edge, but stays adjacent.[14,15] The narrow gap, on the other hand, produces a confluent boundary layer a short distance downstream from the flap leading edge. The gap geometry may be described by the slot flow angle, more physically significant than flap overlap. It is the angle between the slot flow vector and the main wing chord line. The slot flow vector is normal to the minimum radius line from the wing trailing edge to the flap leading edge.

All wind-tunnel tests were conducted at Reynolds number, based on the reference chord, of 2.2×10^6, Mach number of 0.13, and an indicated dynamic pressure of 1150 N/m^2 (24 psf). The transition on the main wing boundary layer was fixed by 2.4-mm-wide trip strips at 5%c upper surface and 10%c lower surface. The test section turbulence level was 1%, as obtained by a single hot-wire probe.

The flow two dimensionality in the test section was evaluated by the visualization of separation patterns on the model upper surface. Tempera and kerosene flow showed a change in the two-dimensional flow character near the sidewalls with the airfoil stalled. Beyond the stall, a spanwise surface flow component within the separated zone appeared and extended toward the juncture of the model and sidewall, where a vortex pair formed and shed at the model trailing edge. However, this was limited to the outer 25% of the span. No boundary-layer control was employed to reduce the three-dimensional flow patterns. The sidewall boundary layer did not have significant effect on the airfoil stall characteristics.[12] This was probably due to the relatively short upstream length of the sidewalls, 1.06 m from the model leading edge. Besides tempera and kerosene, tufts were attached to the model upper surface to supplement the preceding results, and particularly to observe probe interference with the surface flow. The tufts did not show spanwise flow at prestall angles of attack, but at poststall angles it was not clear if the sideway flapping of tufts was due to three dimensionality of the separated flow or the probe interference.

Table 1 Test matrix

	Cases				
	A	B	C	D	E
α, deg	10	0	0	0	0
	15	12.8	12.8	12.8	12.8
	20	15.5	15.5	15.5	15.5
δ, deg	0	30	30	40	40
G/c	—	0.03	0.02	0.015	0.0115
O/c	—	0	0	−0.01	−0.007

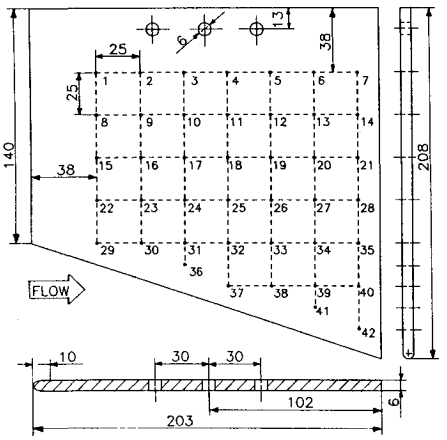

Fig. 2 Pressure port locations on the splitter plate, mm.

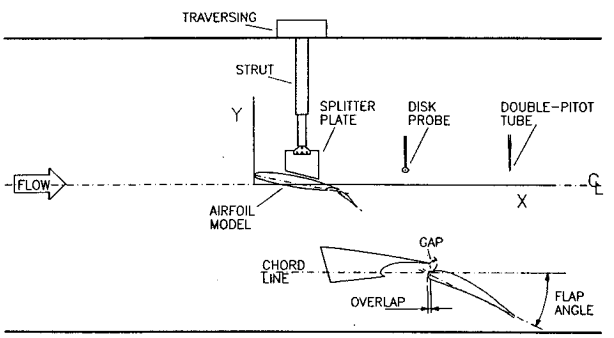

Fig. 3 Sideview of probe and flap positioning in WSU 7×10 ft wind tunnel.

Flowfield was also visualized by using an aluminum splitter plate (not to be confused with the pressure splitter plate described subsequently). The plate was 6.35 mm thick and 610 mm long, extending downstream from the model trailing edge as much as 305 mm. The lower edge of the plate was contoured with the airfoil upper surface. It was supported by a flap hinge and an end plate and mounted at 10% of the span, parallel to sidewalls. Oil dots were placed on grid points 25.4 mm apart on the plate surface. Flow direction at each grid point was observed from the tunnel ceiling during the runs. However, pictures of the plate with vectored oil dots were taken after the airflow stopped and the plate was removed. This caused some oil flow changes before photographing could be done.

Instrumentation

Pressure Instrumentation

The principal instrument used was the specially designed splitter plate shown in Fig. 2 for mapping the flowfield static pressures. The splitter plate can make many measurements simultaneously in the plane of the plate, by pressure taps on the plate surface. The plate was supported by the tunnel traversing strut, as shown in Fig. 3. It has an elliptical leading edge and rounded bottom edge for good surface flow quality. The slope of the bottom edge is straight rather than curved to get closer to the model curvature at all selected angles of attack. The plate is made of aluminum and has 42 pressure taps on one side. These taps connected to stainless-steel tubes buried in the 6.35-mm-thick plate. The pressure tubes ex-

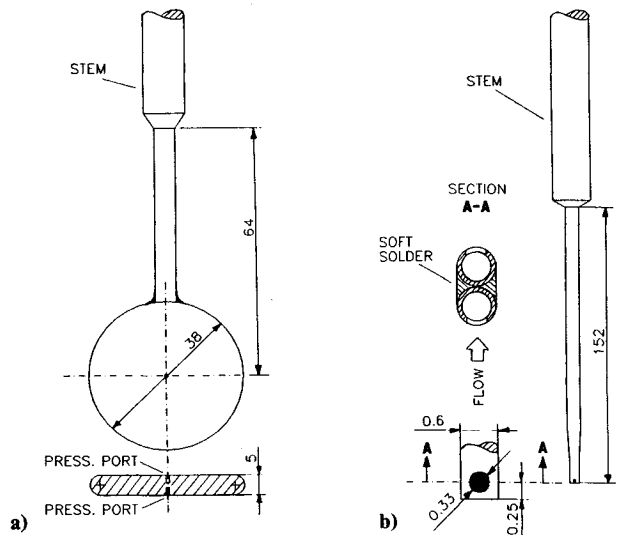

Fig. 4 Pressure probes: a) disk probe and b) double pitot tube, mm.

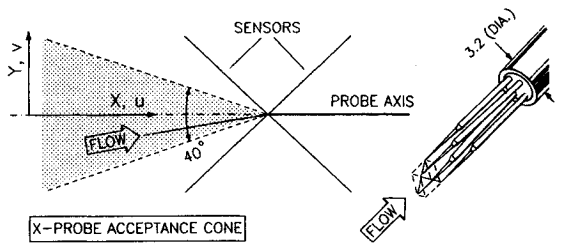

Fig. 5 End flow X-probe with two sensors: 0.051 mm diameter, 90 deg to each other and 45 deg to probe axis, mm.

tended vertically along the traversing strut about 508 mm, and linked to pressure transducers externally, having a resolution of ± 2.4 N/m^2 (0.05 psf). The long tubing length would tend to smooth out any pressure fluctuations, so the pressure readings must be regarded as time-averaged values.

The splitter plate swept the flowfield above and downstream of the model. Starting well above and upstream of the model, the survey was made by moving the plate in 127-mm horizontal (downstream) steps. This made the front two columns of pressure taps overlap the locations of the last two columns of the previous position. After moving downstream of the model, the plate was moved forward and lowered, at most 76 mm. Downstream steps were made again. At least 6.35-mm clearance from the model surface was maintained. When sizable pressure differences were sensed at the same position by the plate overlap at two different steps, the data from the innermost taps on the plate were considered to be the most accurate. Otherwise, data from overlapped taps were averaged. Plate flutter limited the portion of the field that could be measured. It occurred at the most extended, that is, the lowest, strut position when in the wake of the model at high angle of attack. Flutter was monitored visually from the tunnel ceiling window, and no data were used when it was present.

The disk probe, 38 mm diameter and 5 mm thick with a pressure port on the center of each side, as shown in Fig. 4a, was used to supplement the data obtained from the splitter plate. It was initially aligned with the freestream flow by making both sides read the same pressure, with rounded edges for better surface flow quality. The pitot pressure probe with forward and backward facing pressure tubes was used to measure the impact pressure of the axial flow velocity, measured by the hot-film probe described in the following subsection. The probe shown in Fig. 4b was used for previous WSU tests conducted for NASA. Details of the instrumentation and data reduction system for the WSU tests are given in Ref. 16.

Probe interference effects were determined to establish the level of confidence in the measurements of highly separated flows. It was no surprise that probe location had no effect on force and moment values, since only a small part of the span was influenced. Surface pressures showed that the splitter plate and the disk probe interfere with the flow in the plane of measurements only at poststall angles of attack, changing the location of separation point at most 5%c upstream on the model upper surface.

Hot-Film Probe

Flowfield velocity and turbulence quantities were measured by the end flow X-probe hot film (TSI model 1241) shown in Fig. 5, with constant temperature anemometer mode. It consists of two 0.05-mm-diam sensors with platinum film deposited on quartz filament. An overheat ratio of 1.5:1 was used for the measurements. A multichannel digitizer was used for high-speed analog/digital (A/D) conversion of anemometer signals with a sampling rate of 20 kHz per channel and simultaneous A/D conversion. Frequency response of rapid velocity fluctuations was optimized by square wave testing at maximum freestream velocity. This test was done every time the system was activated for measurements. The conditioned signals were visualized by a digital oscilloscope over the period of data acquisition. The signals were interpreted as the turbulence traces of the flowfield and printed out by a plotter. The hot-film probe was calibrated for speed and for yaw angle over a range of ± 25 deg in 5-deg increments. Look-up tables were constructed from the calibration to give flow velocity from the voltage induced by the sensor cooling effect. Calibration was at room temperature, but the hot-film data were corrected for any temperature rise in the wind tunnel.

Results and Discussion

The data obtained by vertical traversing are presented as profiles at the survey stations. The coordinate axis X is defined along the tunnel centerline (positive downstream) passing through the model pivoting location (the half-chord) whereas Y is the coordinate vertical to X axis and tangent to the model leading edge at each angle-of-attack setting ($X = 0$ at the leading edge).

Airfoil Performance

Lift, drag, and moment values were measured by the tunnel balance prior to flowfield measurements and reduced to coefficient forms as C_l, C_d, and C_m. The balance C_l values were compared with those produced by the integration of surface C_p values. Considering all test cases, the integrated value was very close to or at most 4% higher than the balance C_l. Figure 6 shows the increase of lift with flap angle and optimum gap. For the flapped cases, an abrupt loss of lift after the $C_{l_{max}}$ condition is followed by a nearly constant lift and then again a sudden loss. The higher the flap angle, the larger the drop,

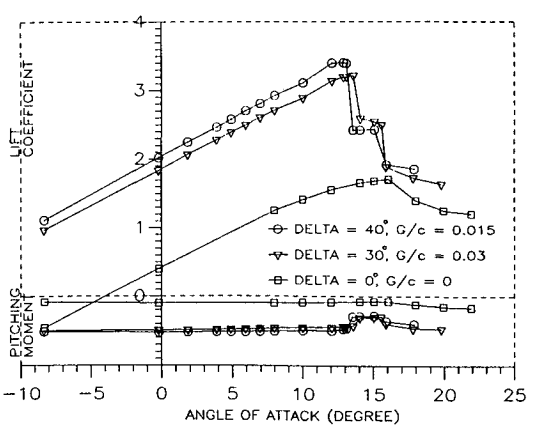

Fig. 6 Effect of flap setting on lift and moment coefficients.

and the wider the flat line appears to be. This interesting feature of the flapped cases was always present and is interpreted as a two-stage stall: stall on the flap and then stall on the wing. Details of this phenomenon and associated hysteresis effects are given in Refs. 13 and 17.

Flowfield Static Pressures

Comparison of the data obtained from the splitter plate and the disk probe was made to determine the credibility of the splitter plate. Both instruments surveyed the same stations, but the disk probe picked data points closer to the model upper surface because of its relatively smaller size. Figures 7 and 8 show the results for test case B at $\alpha = 12.8$ and 15.5 deg, respectively. The data from these probes agree reasonably well at the near-stall angle of attack, but have some discrepancy, seen in Fig. 8 at the poststall angle, especially at the most downward probe positions, where the splitter plate reads higher pressures than the disk probe.

Flowfield static pressures were measured by the splitter plate as described earlier. Results are presented by isobars. These isobars were connected with the airfoil upper surface pressures and left isolated in the far wake regions. They approach the airfoil as nearly orthogonal for the attached flows and parallel for the separated flows. Figures 9 and 10 show the isobars for test case B. At $\alpha = 12.8$ deg, a gradual increase of the streamwise field pressures above the lifting surfaces indicates a favorable condition for the flow to be attached all over the upper surface. The flow accelerated at the leading portion of the airfoil decelerates without any major steepness and reaches the freestream pressure in a relatively short distance downstream. As seen in Fig. 9, freestream pressure is reached at a downward-rearward location. This means that the flap pulls the wing wake downward to increase the airfoil performance at its optimum setting. At $\alpha = 15.5$ deg, there are isobars paralleling the flap and wing upper surface, indicating stall on both the wing and the flap. As the flow becomes separated from the

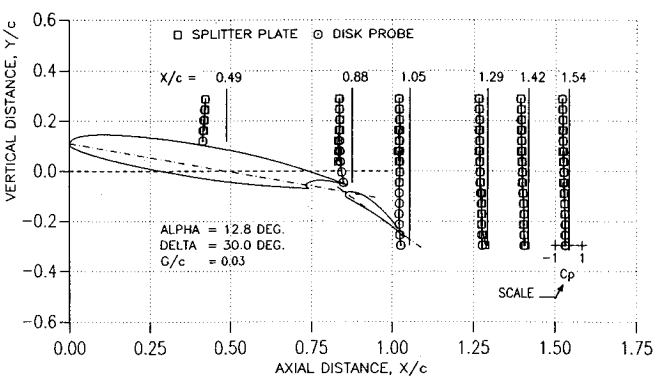

Fig. 7 Comparison of splitter plate and disk probe static pressure coefficients for test case B at $\alpha = 12.8$ deg.

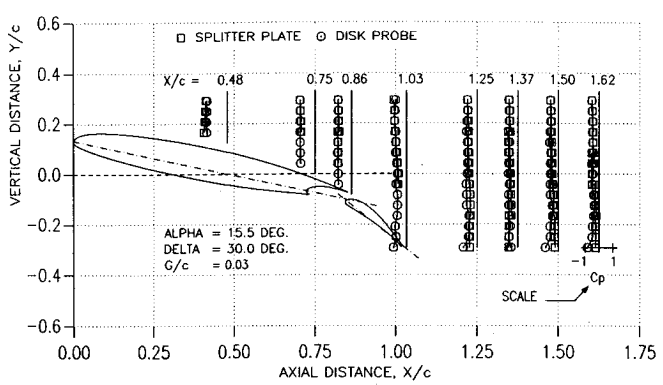

Fig. 8 Comparison of splitter plate and disk probe static pressure coefficients for test case B at $\alpha = 15.5$ deg.

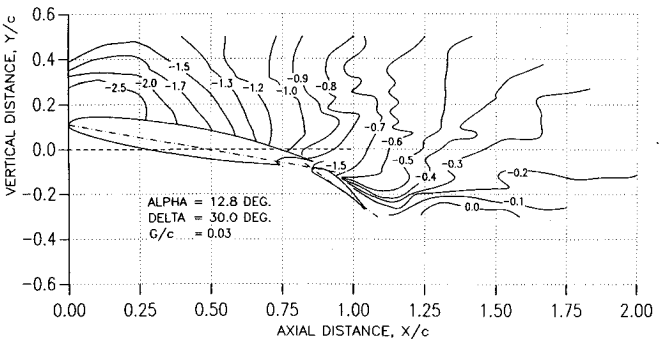

Fig. 9 Flowfield static pressure coefficients contours for test case B at $\alpha = 12.8$ deg.

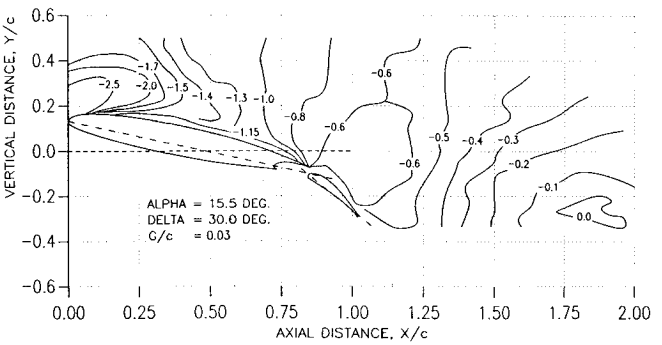

Fig. 10 Flowfield static pressure coefficients contours for test case B at $\alpha = 15.5$ deg.

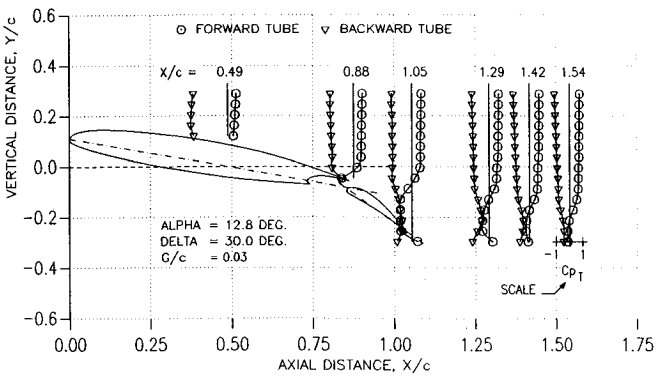

Fig. 11 Pitot pressure coefficients profiles for test case B at $\alpha = 12.8$ deg.

surface, large constant pressure regions seen in Fig. 10 are formed in the flowfield. For the largely separated flowfield, the data do not clearly show the so-called free-stagnation point or saddle point used as an empirical input for analytical wake models, as in Ref. 9, because the region in which the flow tends to stagnate is very sensitive to the probe presence. This is a major difficulty in measuring pressures in separated flows. The presence of a probe, no matter how small, changes the flow geometry in the interacting parts of the flowfield.

Pitot Pressure Profiles

Flowfield total pressures were measured by using the double pitot tube at the survey stations to determine the reverse flow regions. The forward (upstream) and backward (downstream) facing tubes of the measuring probe made simultaneous total pressure measurements at two sides. Total pressure profiles were presented in coefficient form, $C_{p_T} = (p_T - p_\infty)/q_\infty$. The forward and backward pressures reach freestream values at the vertical survey lines.

Figures 11 and 12 show the pitot pressure profiles for test case B at near- and poststall angles of attack. In general, the

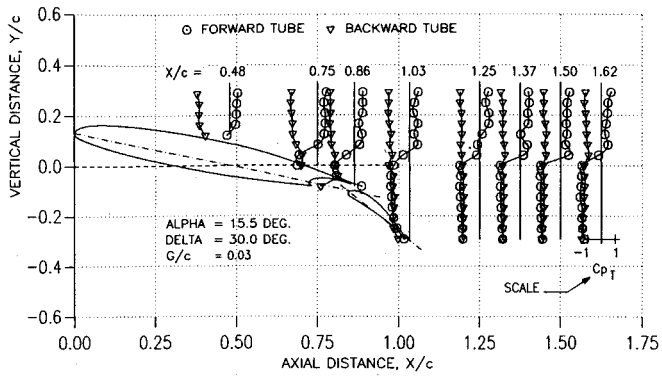

Fig. 12 Pitot pressure coefficients profiles for test case B at $\alpha = 15.5$ deg.

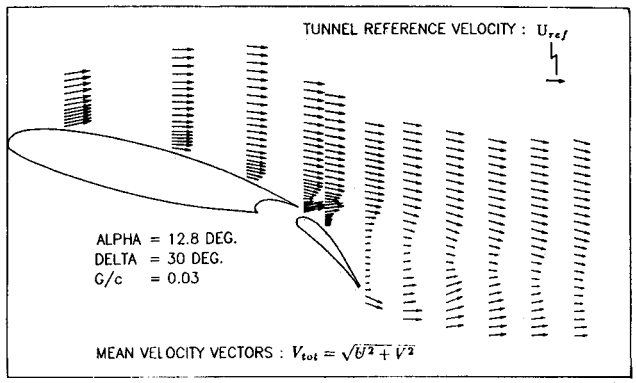

Fig. 13 Mean velocity vector plots for test case B at $\alpha = 12.8$ deg.

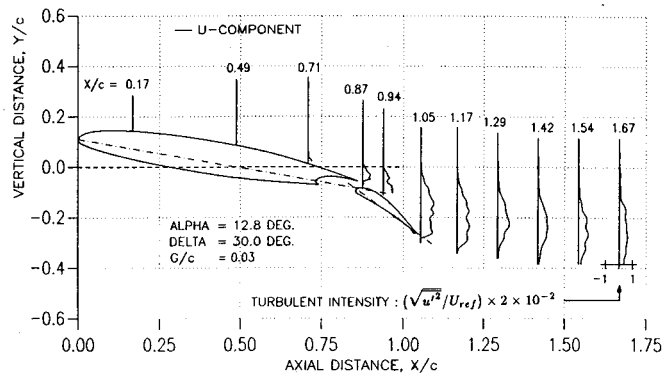

Fig. 14 Mean velocity vector plots for test case B at $\alpha = 15.5$ deg.

forward tube readings are positive and the backward tube readings are negative in the regions of forward flows. But as the flow starts slowing down in the wake regions, the forward tube readings decrease while the backward tube readings increase. When there is no significant axial velocity, both sides read about the same pressure as seen in Fig. 11 for $\alpha = 12.8$ deg. This happens just before the stall on the flap. At $\alpha = 15.5$ deg, the stall on the flap is completed and separation moves upstream on the main wing, as seen in Fig. 12. This time there is a backflow in the wake regions and the forward pressures become more negative than the backward ones.

Hot Film Data

Mean velocity and turbulence data were obtained by using the end flow X probe. The measurements were done at 11 stations for 12.8-deg and 12 stations for 15.5-deg angles of attack. All hot-film data were normalized by the freestream velocity and chord length. Here, the results for test case B at near-stall angle of attack are presented in Figs. 13–16. The asymmetric wake and slot flow are visible in these plots. Flow velocity vectors in Fig. 13 show that the highly accelerated flow at the first station gradually decelerates as it moves downstream. The velocity profile at the flap trailing edge experiences the largest deficit. The deficit is recovered at the following downstream wake stations. At $X/c = 0.87$ and 0.94, the slot flow is well represented by the velocity vectors. The size of the accelerated slot flow is directly determined by the gap. The direction of the jetlike flow appears to be upward, different from the surrounding flow vectors. This trend is also visible in other published data[1,7] for test cases with less than 1%c flap overlaps. For the present tests, the flap position produced zero (cases B and C) or negative overlaps (cases D and E), and therefore all test cases had an upward component in slot flow velocity vectors. However, the size of the component changed significantly with gap width and flap angle for the same overlap, due mainly to the changes in the slot flow orientation with the flap setting. The hot-film probe did not respond well to flow reversals. A split-film probe would provide this type of data. However, the double pitot tube data show the region of flow reversals as mentioned earlier.

Flowfield turbulent intensities are presented for profiles of $\sqrt{\overline{u'^2}}$ at the survey stations and shown in Fig. 14. The trends of turbulent intensity profiles are similar to those of the velocity profiles. In both near- and far-wake regions, the turbulent intensity profiles have a maxima in the center of wakes and a minima (close to zero) in the potential flow regions, including the slot flow.

Flowfield normal stresses are presented in the composite profiles of $\overline{u'^2}$ and $\overline{v'^2}$ components at the survey stations and shown in Fig. 15. The flow irregularity is more pronounced in the normal stress profiles than it is in the mean velocity data. This irregularity increases even more with angle of attack and flap angle. In general, $\overline{u'^2}$ component normal stress is larger than $\overline{v'^2}$ component, except at the most downstream station at $X/c = 1.67$. It is interesting to note that the normal stresses in the wake of the flap at $X/c = 1.05$ are quite low compared to those farther downstream. This is because the main wing wake is relatively strong and tends to suppress the flap wake.

Flowfield shear stresses $\overline{u'v'}$ are presented with profiles at the survey stations and shown in Fig. 16. The shear stress is the

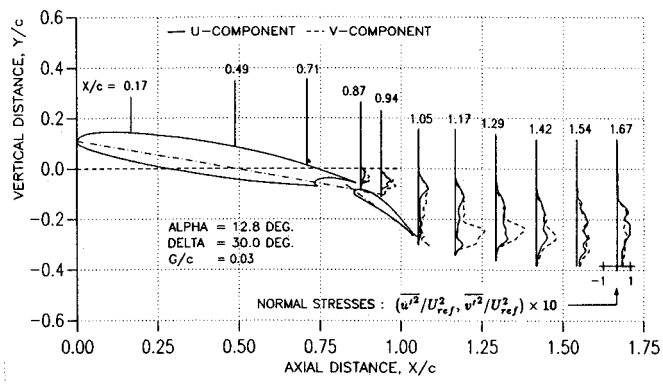

Fig. 15 Normal stress profiles for test case B at $\alpha = 12.8$ deg.

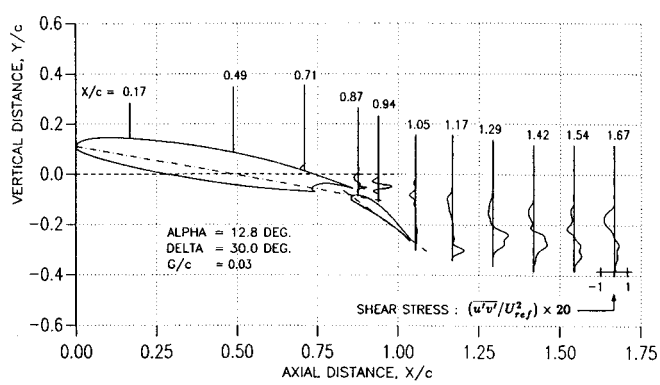

Fig. 16 Shear stress profiles for test case B at $\alpha = 12.8$ deg.

correlation between the fluctuating u' and v' velocity components. The flowfield complexity is quite visible in the shear stress profiles. In the near- and far-wake regions, there are multiple maxima and minima in the profiles. These are the signs of momentum exchange between the high and low momentum parts of the flowfield.

Conclusions

Detailed measurements of pressure, velocity and turbulence quantities have been made above the lifting surfaces and in the near- and far-wake regions of the GA(W)-2 airfoil with 25% single-slotted flap. Based on this experimental study, the following conclusions can be drawn.

1) The specially designed splitter plate proves to be sucessful in measuring a large number of static pressures simultaneously. The plate use was limited only by poststall flutter, a problem preventable by a more rigid plate support system. The disk probe was used for filling the gap in data near the model upper surface. Data from these two pressure instruments agree quite well at stations surveyed. The field pressure data are presented as isobars. These isobars are nearly orthogonal to the lifting surface in the attached flow regions and parallel in the separated flow regions.

2) The flowfield pressure contours do not clearly indicate a pressure peak corresponding to the downstream free-stagnation point, which is the closure of the wake bubble. This is used as an empirical input for analytical separated wake models. Failure to find it is because the stagnation points are very sensitive to the probe presence. This is a difficulty in measuring pressures in separated flows. The presence of a probe, no matter how small, changes the flow geometry in the interacting parts of the flowfield.

3) The shear layer regions were determined by employing the double pitot tube with forward and backward facing tubes. The data clearly show the backflow regions.

4) The end flow X-probe hot-film anemometer was employed to measure mean velocity and turbulence quantities. The data show that the slot flow velocity has an increasing upward component as the slot flow angle increases. This significantly affects the stall characteristics on the airfoil elements.

5) The data presented in this paper are sufficiently detailed to assist in the evaluation of computational codes of separated flows on multielement airfoils.

References

[1]Braden, J. A., Whipkey, R. R., Jones, G. S., and Lilley, D. E., "Experimental Study of the Separating Confluent Boundary Layer," Vol. 1, Summary, NASA CR-3655; Vol. II, Experimental Data, NASA CR-166018, March 1983.

[2]Stevens, W. A., Goradia, S. H., and Braden, J. A., "Mathematical Model for Two-Dimensional Multi-Element Airfoils in Viscous Flow," NASA CR-1843, July 1971.

[3]Olson, L. E., and Orloff, K. L., "On the Structure of Turbulent Wakes and Merging Shear Layers of Multi-Element Airfoils," AIAA Paper 81-1238, June 1981.

[4]Adair, D., and Clifton, H. W., "Turbulent Separated Flow in the Vicinity of a Single-Slotted Airfoil Flap," AIAA Paper 88-0613, Jan. 1988.

[5]Van Den Berg, B., and Oskam, B., "Boundary Layer Measurements on a Two-Dimensional Wing with Flap and a Comparison with Calculations," AGARD CP-271, Sept. 1979.

[6]Brune, G. W., and Sikawi, D. A., "Experimental Investigation of the Confluent Boundary Layer of a Multi-Element Low Speed Airfoil," AIAA Paper 83-0566, Jan. 1983.

[7]Nakayama, A., Kreplin, H.-P., and Morgan, H. L., "Experimental Investigation of Flowfield about a Multielement Airfoil," *AIAA Journal,* Vol. 28, No. 1, 1990, pp. 14–21.

[8]Wentz, W. H., Jr., and Ostowari, C., "Additional Flow Field Studies of the GA(W)-1 Airfoil with 30-Percent Chord Fowler Flap Including Slot-Gap Variations and Cove Shape Modifications," NASA CR-3687, May 1983.

[9]Zumwalt, G. W., and Elangovan, R., "Computation of Low Speed Flow Past Multi-Element Airfoils with Large Flow Separation," *Proceedings of 13th ICAS Congress/AIAA Aircraft Systems and Technology Conference* (Seattle, WA), edited by B. Laschka and R. Staufenbiel, Vol. 1, AIAA, New York, 1982, pp. 342–351.

[10]Wentz, W. H., Jr., "Wind Tunnel Tests of the GA(W)-2 Airfoil with 20% Aileron, 25% Slotted Flap, 30% Fowler Flap and 10% Slot-Lip Spoiler," NASA CR-145139, 1977; also Aeronautical Report 76-2, Wichita State Univ., Wichita, KS, Aug. 1976.

[11]Wentz, W. H., Jr., and Fiscko, K. A., "Pressure Distributions for the GA(W)-2 Airfoil with 20% Aileron, 25% Slotted Flap, 30% Fowler Flap," NASA CR-2948, Feb. 1980.

[12]Wentz, W. H., Jr., and Seetharam, H. C., "Development of A Fowler Flap System for A High Performance General Aviation Airfoil," NASA CR-2443, Dec. 1974.

[13]Biber, K., "Experimental Studies of a Two-Element Airfoil with Large Separation," Ph.D. Dissertation, Dept. of Aerospace Engineering, Wichita State Univ., Wichita, KS, Nov. 1991.

[14]Foster, D. N., Irwin, H. P. A., and Williams, B. R., "The Two-Dimensional Flow around A Single-Slotted Flap," Royal Aeronautical Establishment R&M 3681, Farnborough, England, UK, Sept. 1970.

[15]Smith, A. M. O., "High-Lift Aerodynamics," *Journal of Aircraft,* Vol. 12, No. 6, 1975, pp. 501–530.

[16]Rodgers, E. J., Wentz, W. H., Jr., and Seetharam, H. C., "Instrumentation, Techniques and Data Reduction Associated with Airfoil Testing Programs at Wichita State University," *Advanced Technology Airfoil Research,* Vol. I, NASA CP 2045, Pt. 2, Paper 36, March 1978, pp. 539–558.

[17]Biber, K., and Zumwalt, G. W., "Hysteresis Effects on Wind Tunnel Measurements of a Two-Element Airfoil," *AIAA Journal,* Vol. 31, No. 2, 1993, pp. 326–330.